Journal of Marine Science and Application (2021) 20:706–713
https://doi.org/10.1007/s11804-021-00230-1

RESEARCH ARTICLE

# Blast Pressure Measurements of an Underwater Detonation in the Sea

**Alpaslan Tatlısuluoğlu[1] · Serdar Beji[2]**

Received: 04 May 2021 / Accepted: 16 September 2021 / Published online: 30 November 2021


**Abstract**
Blast pressure measurements of a controlled underwater explosion in the sea were carried out. An explosive of 25-kg trinitrotoluene (TNT) equivalent was detonated, and the blast pressures were recorded by eight different high-performance pressure sensors that work at the nonresonant high-voltage output in adverse underwater conditions. Recorded peak pressure values are used to establish a relationship in the well-known form of empirical underwater explosion (UNDEX) loading formula. Constants of the formula are redetermined by employing the least-squares method in two different forms for best fitting to the measured data. The newly determined constants are found to be only slightly different from the generally accepted ones.

**Keywords** Underwater explosions · High-pressure shock waves · Effects of directionality on blast pressure records · Pressure loading formulas · Applications of the least-squares method

## 1 Introduction

In an underwater detonation, the formation of a superheated and highly compressed gas bubble around the charge causes a tremendous pressure increase which in turn gives rise to a shock wave (Reid 1996). The spherically propagating shock wave initially has a speed much faster than that of the sound in water and a steep front with a sharp peak pressure value well above the acoustic pressure levels, which decays in an approximately exponential fashion. As the gas bubble expands, the pressure inside begins to drop, and the expansion overshoots, reversing the process to a contraction with an increase in pressure again. This cycling repeats itself a few times, generating diminishing pressure pulses, while the bubble rises up toward the surface under the lifting force of hydrostatic pressure. The peak pressure of a shock wave experienced at a relatively closer distance from the charge is of great importance in various cases, the most important being an explosion in the vicinity of a submarine or surface ship.

Due to confidentiality concerns, field measurements of controlled underwater explosions are rarely reported in the open literature; the studies usually concentrate on numerical simulations, and to a lesser extent, on experimental measurements in laboratory conditions. Kwon and Fox (1993) studied experimentally and numerically the shock response of a cylinder to a far-field underwater explosion. Zhao et al. (2003) employed a finite element analysis software to model the shock resistance performance of a floating raft. Shin (2004) used a commercial code for a three-dimensional ship shock simulation and compared the results with actual test data. Ramajeyathilagam and Vendhan (2004) conducted experiments and numerically modeled the thin rectangular plates under blast loading, while Hung et al. (2005) did quite similar work for aluminum plates. Yao et al. (2007) mathematically analyzed the interaction of two bubbles generated by an underwater explosion. Based on the energy method, Peng et al. (2009) developed a formula for estimating plastic deformation of the protective bulkhead of

**Article Highlights**
- Pressure measurements of an underwater explosion in the sea are done at eight different gauges.
- Effects of directionality on blast pressures are observed for gauges at equal distances from the charge but in different directions.
- Coefficients of underwater explosion loading formula are redetermined by the use of measured peak pressure values.
- Two different error functions are employed in the application of the least-squares method for determining the coefficients of the loading formula.

✉ Alpaslan Tatlısuluoğlu
tatlisuoglu@yahoo.com

[1] Ph. D. student at I. T. U. and Underwater Search and Rescue Command, TR-34469 Istanbul, Turkey

[2] Faculty of Naval Architecture and Ocean Engineering, Istanbul Technical University, TR-34469 Istanbul, Turkey

a warship under blast loading. Li et al. (2011) conducted underwater explosion trials using unfilled and sand-filled cylindrical shells to determine elastic and plastic deformations. Barras et al. (2012) numerically modeled the bubble dynamics in an underwater explosion. Cavitation effects on ships were studied by Zong et al. (2012). Emamzadeh et al. (2015) considered the propagation of explosion waves to far fields and their effects on structures. The response of a multilayered structure to shock waves was experimentally investigated by Zhang et al. (2017). Brochard et al. (2019) worked on the development of a simplified analytical method for estimating the structural response of an immersed cylinder subjected to an underwater explosion. Camargo (2019) summarized the mathematical formulations for the damage prediction of naval panels. Hawass et al. (2019) theoretically and experimentally analyzed the performances of various underwater explosive compositions. Directional effects in underwater explosions were studied by Huang et al. (2019). Gan et al. (2021) evaluated the deformation characteristics of a floating slender structure due to UNDEX. Jiang et al. (2021) performed trials of shock wave effects on thin-walled aluminum plates. Numerical simulations of structural damage due to near-field underwater explosions were carried out by Peng et al. (2021).

Setting up a detonation experiment and carrying out measurements at sea are major difficulties in conducting a controlled underwater test in the field. This work precisely takes up this challenging task and reports the pressure measurements recorded during a planned underwater detonation carried out in open sea. Peak pressure measurements are used to redetermine the coefficients of a well-known heuristic formula expressing the maximum pressure as a function of charge quantity and standoff. Comparing the newly determined coefficients with the generally assumed values reveals only slight differences, bolstering confidence in both the formula and measurements.

## 2 Open-Sea Detonation Measurements

Pressure measurements were carried out during a planned open-sea underwater detonation. Time histories of pressure changes in water were recorded at eight stations placed at different locations. Evaluation of measurements and use of peak-pressure values for redetermining the coefficients of the empirical power-law approximation (Cole 1948) are given in this section; but first, some general information on the underwater explosions is presented.

### 2.1 Underwater Explosion Process

Explosions transform energy from one form to several other forms in a relatively short period of time and space with a strong mechanical effect. An underwater explosion, typically initiated by detonating a highly explosive material, leads to a complex sequence of events. The explosive, a chemically unstable substance, is triggered into a chemical reaction which results in the explosion. The unstable substance is converted into a stable gas at a very high temperature (~3000°C) and pressure (~50000 atm) (Cole 1948). Almost instantaneous rise of pressure to a peak value in the superheated gas generates a compression wave with a steep wall-like front and exponentially decaying back, propagating radially (Reid 1996). This is called the shock wave, and it is the most destructive one among a series of pulses generated by an underwater explosion. Typically, 53% of the released energy is depleted for generating the shock wave, while the remaining 47% is used for the formation of the secondary pulses that follow the shock wave (Hsu et al. 2014). The propagation velocity of the shock wave initially exceeds the speed of sound in water (~1500 m/s) by a factor of several times but quickly falls to this value as the wave propagates and the pressure drops to the acoustical levels. At first, the dropping of the pressure with distance is faster than the inverse-first-power-law, but as the wave amplitude diminishes with further outward propagation, the inverse-first-power-law establishes itself for the pressure fall.

Besides the reflections of a shock wave from the free surface and seabed, cyclic overshooting and receding phases of the gas bubbles give rise to successive secondary pressure pulses. The peak pressure in the first bubble pulse is only 10% to 20% of the primary shock wave, but the pulse duration is longer, thus making the areas under the two pressure-time curves quite nearly the same. Successive pulses get lower and lower in strength, and generally, it is the first secondary pulse that is of any practical concern.

A detailed account of all these processes and the Kirkwood–Bethe theory, covering the first analytical treatment of finite-amplitude shock-wave propagation, can be found in Cole (1948).

### 2.2 Field Measurements

An underwater detonation with eight pressure gauges, mounted on a suspended steel frame in the seawater was carried out. A cylindrical explosive of a 25-kg TNT equivalent was detonated in the sea at 18 m depth, where the total water depth was 30 m. The cylindrical charge had a radius of $r = 190$ mm and a length of $l = 49$ mm. The time histories of issuing pressure variations were recorded by non-resonant, high-voltage output, PCB series pressure sensors. An L-shaped steel frame suspended by buoyant spheres was used to hold the pressure gauges at different positions as shown in Figure 1. Gauges 1–7 were placed on the same plane, say $y - z$ plane, at different distances and positions, while a single gauge, number 8, was placed on the $x - z$

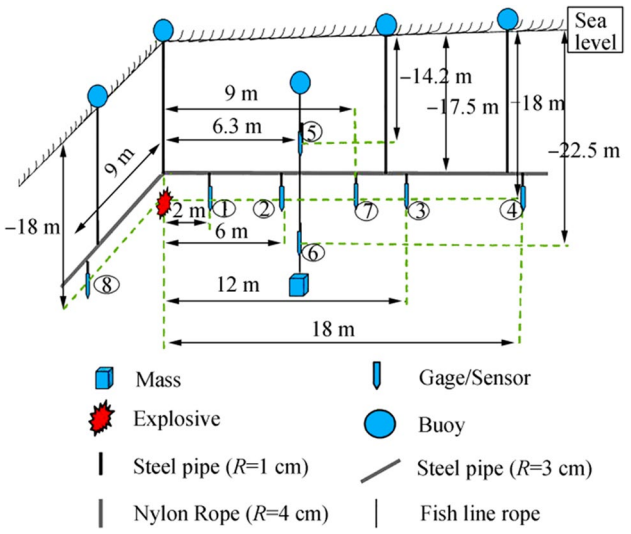


**Figure 1** Schematic description of locations of charge and pressure gauges for underwater detonation

plane at a distance of 9 m. from the charge, serving as the counterpart of gauge 7 of the $y-z$ plane. The closest possible distance for the location of the first pressure sensor, gauge 1, was determined by ensuring that the sensor could withstand the peak pressure without breaking down. The standoff for the remotest sensor, gauge 4, was selected by giving a good allowance for a clear observation of the exponential decay. Three of the remaining sensors, gauges 2, 3, and 7, were placed in between gauges 1 and 4. Two of the sensors, gauge 5 and 6, were placed between gauges 4 and 7, above and below the reference depth 18 m for seeing the depth effect, if any. Finally, the last sensor, gauge 8, was placed in a direction at a right angle to the others to observe the effect of directionality. Considering the weather conditions and forecasts, the test day was selected to ensure a calm sea state with minimum disturbance from the waves. Fishline ropes were used to fix the sensors effectively; once the entire frame was afloat in the sea, the divers checked and made sure the correct positions of the sensors prior to the detonation.

Figure 2 shows the time records of pressure sensors in the order of their distances from the charge, starting from the nearest, $R = 2$ m, gauge 1 ending with $R = 18$ m gauge 4. Note also that since there are big differences in the maximum pressure values, three different vertical scales are used to give a clearer view of each record. Different characteristics of the secondary pulses for each sensor are the most noteworthy aspect of these records. Besides, the pulsations of the primary bubble, reflections, and re-reflections from the seabed and the free surface play an important part in establishing the characteristics of the secondary peaks. Note also that the shown pressure values are the gauge pressures zero-referenced against the ambient pressure, hence the pulse-like motions of the explosion bubble and reflections from the bottom and free surface cause apparent below-zero pressure values as well as differences in pressure curves.

Both the shock wave peak pressure and the impulse, the latter being directly related to peak pressure and pulse duration, are very important parameters for assessing the potential damage to a sea structure. Pulse duration itself carries additional importance as it might trigger resonance, depending on the eigen period of the structure. Table 1 presents the measured peak pressure values and the corresponding distances from the charge for all the gauges. Gauge 7 and 8 both have a 9 m distance from the charge; only their direction is different. On the other hand, the maximum shock wave pressures measured by these gauges differ from each other by approximately 18%. Besides, this notable difference in the peak pressure values, the time histories in the low-pressure parts caused by bubble contractions, differs appreciably. All these differences in both the peak values and below-zero pressure fluctuations indicate variabilities that could be induced by directionality. Note that gauge 8 has consistently higher peak pressure and lower below zero levels compared to gauge 7. More specially, imperfect symmetry in an explosion gives rise to such different maxima and minima in different directions and that these maxima and minima are proportional. Huang et al. (2019) examined this rather less-studied subject of directional effects in underwater explosions by conducting experiments and performing numerical simulations.

## 3 Shock Wave Pressure Loading

A shock wave causes an almost instantaneous (less than $10^{-7}$ s) rise of pressure to a peak value which decays in time nearly in an exponential fashion. A well-known semiempirical formula describing the exponential decay is given by (Cole 1948; Keil 1961).

$$p(t) = p_{\mathrm{m}} e^{-t/\theta} \tag{1}$$

where $p(t)$ is the instantaneous pressure, $p_{\mathrm{m}}$ the peak pressure, $t$ the time, and $\theta$ the decay time that the pressure drops to $1/e$ of the peak value, $p(\theta) = p_{\mathrm{m}}/e$. Equation (1) is valid for $0 \le t \le \theta$. The peak or maximum pressure $p_{\mathrm{m}}$ and decay time would obviously depend on the quantity of charge and the distance from this charge at which the observation is done. $p_{\mathrm{m}}$ and $\theta$ are expressed by the following empirical relations (Cole 1948; Keil 1961):

$$p_{\mathrm{m}} = k_1 \left( \frac{W^{1/3}}{R} \right)^{\alpha_1} \tag{2}$$

$$\theta = k_2 W^{1/3} \left( \frac{W^{1/3}}{R} \right)^{\alpha_2} \tag{3}$$

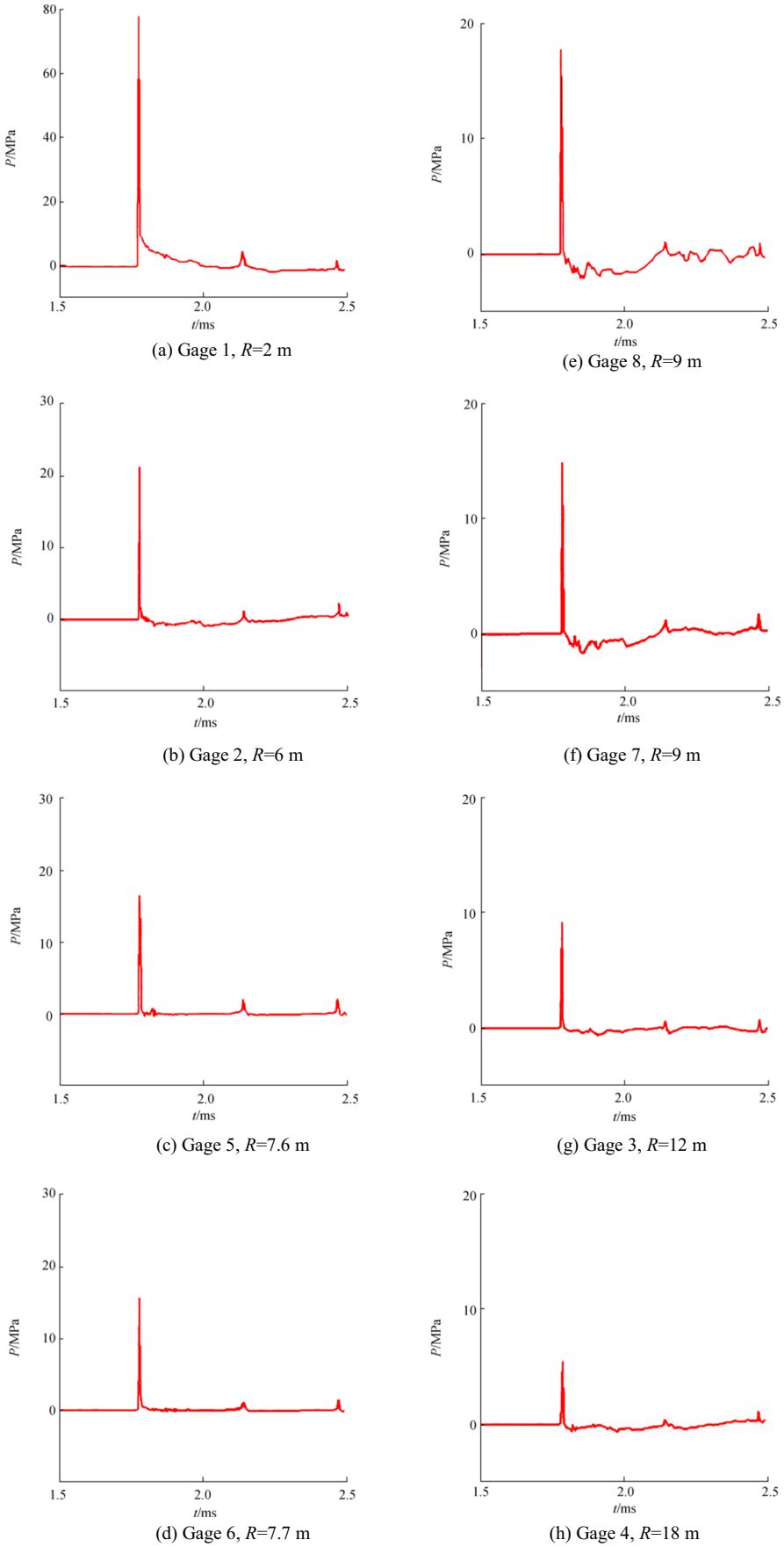


**Figure 2** Blast pressure versus time as recorded by gauges, given in the order from the highest to the lowest peak pressure. **a** Gauge 1, $R = 2$ m; **b** Gauge 2, $R = 6$ m; **c** Gauge 5, $R = 7.6$ m; **d** Gauge 6, $R = 7.7$ m; **e** Gauge 8, $R = 9$ m; **f** Gauge 7, $R = 9$ m; **g** Gauge 3, $R = 12$ m; **h** Gauge 4, $R = 18$ m

in which the explosive quantity $W$ is defined in terms of the equivalent amount of TNT and $R$ is standoff with $k_1$, $\alpha_1$, and $k_2$, $\alpha_2$ denoting the tuning parameters.

The well-established and most frequently used coefficients are given as $k_1 = 21600$, $\alpha_1 = 1.13$, and $k_2 = 0.058$, $\alpha_2 = -0.22$ when $p_m$ is in psi and $\theta$ in millisecond (Keil 1961). When the quantities are expressed in SI units,

$$p_m = 52.4\left(\frac{W^{1/3}}{R}\right)^{1.13} \tag{4}$$

$$\theta = 92.5W^{1/3}\left(\frac{W^{1/3}}{R}\right)^{-0.22} \tag{5}$$

where $p_m$ is in megapascal (MPa), $W$ in kilogram (kg), $R$ in meter (m), and $\theta$ in microsecond (μs). In this work, the above expressions with given coefficients are referred to as the standard formulas since they are conventionally the most preferred ones.

Zamyshlyaev and Yakovlev (1973) gave a redefined version of the peak pressure Eq. (4):

$$\begin{aligned} p_m &= 44.1\left(\tfrac{W^{1/3}}{R}\right)^{1.5} \text{for } 6 < \tfrac{R}{r} < 12 \\ p_m &= 52.4\left(\tfrac{W^{1/3}}{R}\right)^{1.13} \text{for } 12 \le \tfrac{R}{r} < 240 \end{aligned} \tag{6}$$

where $r$ is the radius of charge, and all the units are as indicated for Eq. (4). Note that the refinement is introduced only in the near field $6 < R/r < 12$, while the far-field expression is kept the same as (4).

## 4 Redetermination of Coefficients from Measured Peak Pressure Values

Using the measured data given in Table 1, the coefficients $k_1$ and $\alpha_1$ in Eq. (2) are redetermined by the method of the least-squares (Ralston and Rabinowitz 2001). Following the usual approach first, we take the natural logarithm of Eq. (2):

**Table 1** Measured shock wave peak pressure values and distances to charge

| Gauge number | Distance from charge $R$ (m) | Measured maximum pressure $p_m$ (MPa) |
|---|---|---|
| 1 | 2.0 | 77.48 |
| 2 | 6.0 | 21.13 |
| 3 | 12.0 | 9.05 |
| 4 | 18.0 | 5.47 |
| 5 | 7.6 | 16.34 |
| 6 | 7.7 | 15.53 |
| 7 | 9.0 | 14.82 |
| 8 | 9.0 | 17.76 |

$$\ln\ p_m = \ln\ k_1 + \alpha_1 \ln\left(\frac{W^{1/3}}{R}\right) \tag{7}$$

The total error as defined by the squares of differences between the measured and the predicted pressure values is as follows:

$$E^2(k_1, \alpha_1) = \sum_{i=1}^{N}\left[\ln\ p_{m_i} - \ln\ k_1 - \alpha_1 \ln\left(\frac{W^{1/3}}{R_i}\right)\right]^2 \tag{8}$$

in which $N$ stands for the total number of data points. The least-squares method aims at minimizing the total error by appropriately selecting the parameters involved. To accomplish this aim, the error function $E^2(k_1, \alpha_1)$ is differentiated with respect to $k_1$ and $\alpha_1$, separately, and the resulting expressions are set to zero. Thus, for the determination of $\ln k_1$ and $\alpha_1$, the following linear equations are obtained.

$$N\ \ln k_1 + \alpha_1 \sum_{i=1}^{N}\left(\frac{W^{1/3}}{R_i}\right) = \sum_{i=1}^{N} \ln\ p_{m_i} \tag{9}$$

$$\ln\ k_1 \sum_{i=1}^{N} \ln\left(\frac{W^{1/3}}{R_i}\right) + \alpha_1 \sum_{i=1}^{N}\left[\ln\left(\frac{W^{1/3}}{R_i}\right)\right]^2 = \sum_{i=1}^{N} \ln\ p_{m_i} \ln\left(\frac{W^{1/3}}{R_i}\right) \tag{10}$$

Taking $W = 25$ kg and using all the measured, $N = 8$, peak pressure values $p_{mi}$ and corresponding standoffs $R_i$ listed in Table 1 in the above equations give $k_1 = 51.5$ and $\alpha_1 = 1.18$ as solutions. These values are quite comparable with the generally accepted $k_1 = 52.4$ and $\alpha_1 = 1.13$ values. Note that numerically higher powers such as $\alpha_1 = 1.16$ (Cole 1948) and $\alpha_1 = 1.18$ (Shin 2004) were also reported for TNT.

At this point, we should like to diverge from the usual approach slightly and do the least-squares analysis by using the approximating function for $p_m$ directly without introducing the logarithm. The total error for this case is simply,

$$E^2(k_1, \alpha_1) = \sum_{i=1}^{N}\left[p_{mi} - k_1\left(\frac{W^{1/3}}{R_i}\right)^{\alpha_1}\right]^2 \tag{11}$$

Differentiating Eq. (11), with respect to $k_1$ and $\alpha_1$, in turn, gives the following equations for obtaining $k_1$ and $\alpha_1$.

$$k_1 \sum_{i=1}^{N}\left(\frac{W^{1/3}}{R_i}\right)^{2\alpha_1} = \sum_{i=1}^{N} p_{m_i}\left(\frac{W^{1/3}}{R_i}\right)^{\alpha_1} \tag{12}$$

$$k_1 \sum_{i=1}^{N}\left(\frac{W^{1/3}}{R_i}\right)^{2\alpha_1} \ln\left(\frac{W^{1/3}}{R_i}\right) = \sum_{i=1}^{N} p_{m_i}\left(\frac{W^{1/3}}{R_i}\right)^{\alpha_1} \ln\left(\frac{W^{1/3}}{R_i}\right) \tag{13}$$

Obviously, solving $k_1$ and $\alpha_1$ from the above equations is not a straightforward task and that is the reason the logarithmic formulation is used routinely. Nevertheless, it is possible

to devise an approach to extract the solutions. $\alpha_1$ is assigned a range of values between 1.0 and 2.0 by small increments such as $\Delta\alpha = 10^{-5}$ while $k_1$ is computed separately from Eqs. (12) and (13) for each $\alpha_1$ value. The difference between two $k_1$ values, as computed from (12) and (13), is checked at every step until it gets less than a preset small value such as $10^{-3}$. When this criterium is satisfied, the $\alpha_1$ value used at that particular step and the average of two corresponding $k_1$ values are taken as solutions. Again, using the data of Table 1, with $N = 8$ points, the computations yield $k_1 = 50.3$ and $\alpha_1 = 1.14$ from Eq. (12) and (13). Albeit slightly, these values are different from the solutions obtained from the usual approach given by (9) and (10). Note that $\alpha_1$ is now much closer to the generally adopted value 1.13.

We should now comment on the reason for differences in the coefficients in these slightly different applications of the least-squares method. Equation (8) computes the logarithmic errors, which are not the same as the direct errors of Eq. (11) since the logarithm function is not a linear operation. As the errors minimized are not the same, the computed coefficients are different. In this respect, the second approach that minimizes the direct errors is obviously better as it uses the actual total error between the measured and computed pressure values. Numerically, the total error for each case can be computed by using the direct error defined in (11). If this is done, the first approach with $k_1 = 51.5$ and $\alpha_1 = 1.18$ gives $E^2(k_1, \alpha_1) = 30.59$, while the direct approach with $k_1 = 50.3$ and $\alpha_1 = 1.14$ gives $E^2(k_1, \alpha_1) = 19.65$, which is lower than the former.

Figure 3 shows the measured peak pressure data against the plots of the power-law formula (2) for three different sets of coefficients: the standard or generally used parameters $k_1 = 52.4$, $\alpha_1 = 1.13$, the logarithmic approach results $k_1 = 51.5$, $\alpha_1 = 1.18$, and finally the direct approach $k_1 = 50.3$, $\alpha_1 = 1.14$. Overall, only minor differences can be observed from Figure 3; however, a closer view and comparisons with measurements for each $k_1$, $\alpha_1$ pair reveal clearly that the error minimization done by the direct use of the power function results in the least errors for the data points used (Table 2). Measurements done by Hung et al. (2005) in the laboratory give these coefficients as $k_1 = 59.5$, $\alpha_1 = 1.29$, which are appreciably different from the values obtained here. Naturally, there are notable differences between the open sea and laboratory conditions. The most obvious one is the relatively large domain of the sea compared to the small and enclosed region of the laboratory. Due to stronger reflection effects in confined regions, even the scaled measurements would not agree perfectly with those recorded in an open environment. The difference in bottom material is another important point related to reflection and differences in measurements in the sea with relatively soft bottom material such as mud and in the laboratory with concrete base are quite normal. Bias caused by environmental effects like

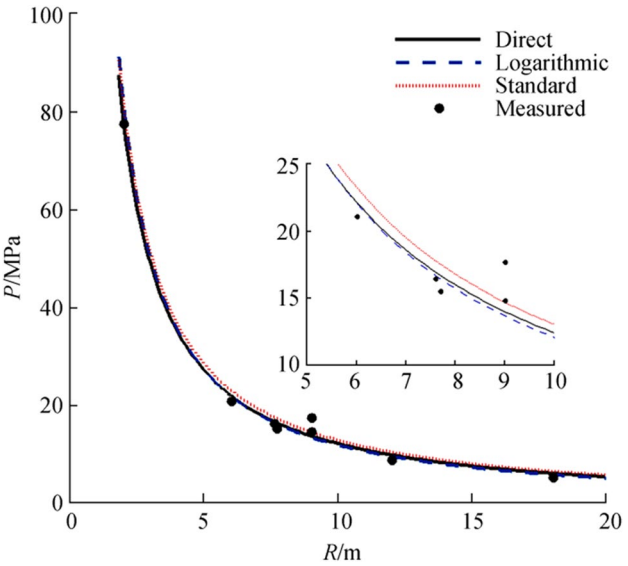


**Figure 3** Measured peak pressure values and the power-law formula with different coefficients

waves and currents must too be borne in mind. In the same vein, equipment and its deployment in the ocean require more durability and care. We may then conclude that all these reasons contribute to the differences in parameters determined according to measurements performed in the open sea and laboratory.

In terms of the newly determined $k_1$, $\alpha_1$ pair, we have

$$p_m = 50.3\left(\frac{W^{1/3}}{R}\right)^{1.14} \tag{14}$$

where $p_m$ is in pascal as indicated before. We remark that the performance of the present Eq. (14) is very close to that of the standard one; slight differences observed between the customary loading formula, and the new measurements may be attributed to two main reasons. First, the well-known

**Table 2** Measured shock wave peak pressure values compared with computed predictions from different $k_1$ and $\alpha_1$

| Standoff $R$ (m) | Measured | Direct $p_m$ | Logarithmic (MPa) | Standard |
|---|---|---|---|---|
| 2.0 | 77.48 | 77.42 | 80.65 | 80.49 |
| 6.0 | 21.13 | 22.18 | 22.08 | 23.26 |
| 7.6 | 16.34 | 16.95 | 16.71 | 17.81 |
| 7.7 | 15.53 | 16.70 | 16.46 | 17.55 |
| 9.0 | 14.82 | 13.99 | 13.69 | 14.71 |
| 9.0 | 17.76 | 13.99 | 13.69 | 14.71 |
| 12.0 | 9.05 | 10.08 | 9.75 | 10.63 |
| 18.0 | 5.47 | 6.36 | 6.05 | 6.72 |

loading formula is the outcome of a curve fitting to a definite measured data which has deviations from the curve itself. Second, the sensors used in the present work are of the newest type with better technical capabilities.

Restricted access to the measurement data does not allow the determination of decay time; therefore, the constants $k_2$ and $\alpha_2$ in Eq. (3) could not be computed.

## 5 Concluding Remarks

Blast pressure measurement records of a controlled underwater explosion in the sea have been presented. Besides confidentiality issues, installation, deinstallation, equipment durability, and overall expenditures are burdensome matters in ocean measurements that require much care, planning, and involvement of a professional maritime team with scuba divers. Ensuring the correct positions of the sensors alone is a tedious task in itself. For all these and more reasons, the reported actual sea trials are rare and the value of actual field data cannot be overestimated. The measurements reported here are expected to be useful not only for confirming previous works but also for testing the relevant numerical simulations.

In the mathematical part of the work, parameters of the semiempirical maximum pressure formula are redetermined by the use of field data by employing two different formulations of the error function. The first formulation is the classical way of applying the least-squares method to an exponential function by employing the logarithmic approach. On the other hand, the second formulation is entirely new and uses the error function directly without resorting to any additional manipulation. Therefore, the latter approach might be viewed as rendering the true minimum of the total errors. Calculated coefficients from two different approaches show slight variations depending on the error function adopted but agree fairly well with the generally accepted values. This agreement serves as a further assurance of the accuracy of measurements.

**Acknowledgements** This work was carried out as a part of doctoral studies of the first author at Istanbul Technical University.

## References

Barras G, Souli M, Aquelet N, Couty N (2012) Numerical simulation of underwater explosions using an ALE method The pulsating bubble phenomena. Ocean Eng 41:53–66. https://doi.org/10.1016/j.oceaneng.2011.12.015

Brochard K, Sourne HL, Barras G (2019) A simplified method to assess the damage of a deeply immersed cylinder subjected to underwater explosion. Int J Saf Secur Eng 9(2):95–108

Camargo FV (2019) Survey on experimental and numerical approaches to model underwater explosions. J Mar Sci Eng 7(1):15. https://doi.org/10.3390/jmse7010015

Cole RH (1948) Underwater explosions. Princeton University Press, Princeton

Emamzadeh SS, Ahmadi MT, Mohammadi S, Biglarkhani M (2015) Dynamic adaptive finite element analysis of acoustic wave propagation due to underwater explosion for fluid-structure interaction problems. J Mar Sci Appl 14:302–315. https://doi.org/10.1007/s11804-015-1322-x

Gan N, Liu LT, Yao XL, Wang JX, Wu WB (2021) Experimental and numerical investigation on the dynamic response of a simplified open floating slender structure subjected to underwater explosion bubble. Ocean Eng 219:108308. https://doi.org/10.1016/j.oceaneng.2020.108308

Hawass A, Elbeih A, Mostafa HE (2019) Theoretical and experimental study of underwater explosion performance of selected explosive compositions. 18th International Conference on Aerospace Sciences & Aviation Technology, IOP Conf. Series: Materials Science and Engineering, 610, 012061

Hsu CY, Liang CC, Teng TL, Nguyen HA (2014) The study on the underwater shock loading empirical formula. https://www.researchgate.net/publication/281823479 [Accessed on 21 Sept 2021]

Huang C, Liu M, Wang B, Zhang Y (2019) Underwater explosion of slender explosives: directional effects of shock waves and structure responses. Int J Impact Eng 130:266–280. https://doi.org/10.1016/j.ijimpeng.2019.04.018

Hung CF, Hsu PY, Hwang-Fuu JJ (2005) Elastic shock response of an air-backed plate to underwater explosion. Int J Impact Eng 31(2):151–168. https://doi.org/10.1016/j.ijimpeng.2003.10.039

Jiang X, Zhang W, Li D, Chen T, Tang C, Guo Z (2021) Experimental analysis on dynamic response of pre-cracked aluminum plate subjected to underwater explosion shock loadings. Thin Walled Struct 159:107256. https://doi.org/10.1016/j.tws.2020.107256

Keil AH (1961) The response of ships to underwater explosions. Trans Soc Naval Archit Mar Eng 69:366–410

Kwon YW, Fox PK (1993) Underwater shock responses of a cylinder subjected to a side-on explosion. Comput Struct 48(4):637–646

Li LJ, Jiang WK, Ai YH (2011) Experimental study on dynamic response and shock damage of cylindrical shell structures subjected to underwater explosion. J Offshore Mech Arct Eng 133(1):011102

Peng X, Nie W, Yan B (2009) Capacity of surface warship's protective bulkhead subjected to blast loading. J Mar Sci Appl 8:13–17. https://doi.org/10.1007/s11804-009-8012-5

Peng YX, Zhang AM, Ming FR (2021) Numerical simulation of structural damage subjected to the near-field underwater explosion based on SPH and RKPM. Ocean Eng 222:108576. https://doi.org/10.1016/j.oceaneng.2021.108576

Ralston A, Rabinowitz P (2001) A first course in numerical analysis. Dover Publications, Inc., Mineola, New York

Ramajeyathilagam K, Vendhan JP (2004) Deformation and rupture of thin rectangular plates subjected to underwater shock. Int J Impact Eng 30:699–719. https://doi.org/10.1016/j.ijimpeng.2003.01.001

Reid WD (1996) The response of surface ships to underwater explosions. DSTO Aeronautical and Maritime Research Library, Melbourne, Victoria, Australia

Shin YS (2004) Ship shock modeling and simulation for far-field underwater explosion. Comput Struct 82:2211–2219. https://doi.org/10.1016/j.compstruc.2004.03.075

Yao X, Zhang A, Liu Y (2007) Interaction of two three-dimensional explosion bubbles. J Mar Sci Appl 6(2):12–18. https://doi.org/10.1007/s11804-007-6058-9

Zamyshlyaev B, Yakovlev Yu S (1973) Dynamic loads in underwater explosion. Naval Intelligence Support Center, Washington D. C. (Translated from Russian, Dinamicheskiye nagruzki v podvodnom vzryve, Sudostroyeniye, Leningrad, 1967)

Zhang J, Shia XU, Guedes Soares C (2017) Experimental study on the response of multi-layered protective structure subjected to underwater contact explosions. Int J Impact Eng 100:23–34

Zhao Y, He L, Huang Y, Wang Y (2003) FEA for designing of floating raft shock-resistant system. J Mar Sci Appl 2(1):24–28. https://doi.org/10.1007/BF02935571

Zong Z, Zhao Y, Ye F, Li H, Chen G (2012) Parallel computing of the underwater explosion cavitation effects on full-scale ship structures. J. Mar Sci Appl 11:469–477. https://doi.org/10.1007/s11804-012-1157-7